Dispersion and Reduction of Copper Oxide Supported on WO_3-Modified $Ce_{0.5}Zr_{0.5}O_2$ Solid Solution

Li Xiaowei,[†] Shen Mingmin,[†] Hong Xi,[†] Zhu Haiyang,[†] Gao Fei,[†] Kong Yan,*[,‡] Dong Lin,*[,†] and Chen Yi[†]

Key Laboratory of Mesoscopic Chemistry, Department of Chemistry, Nanjing University, Nanjing 210093, People's Republic of China, and College of Chemistry and Chemical Engineering, Nanjing University of Technology, Nanjing 210009, People's Republic of China

Received: July 22, 2004; In Final Form: November 4, 2004

XRD (X-ray diffraction), BET (Brunauer−Emmett−Teller), LRS (laser Raman spectra), XPS (X-ray photoelectron spectroscopy), and TPR (temperature-programmed reduction) are used to investigate the surface properties of $CuO/WO_3/Ce_{0.5}Zr_{0.5}O_2$ samples. The results indicate that (1) tungsten oxide can be highly dispersed on $Ce_{0.5}Zr_{0.5}O_2$ (denoted as CZ hereafter) solid solution, with a dispersion capacity of about 0.8 mmol WO_3/(100 m^2 CZ), and comparatively, the supported tungsten oxide species are preferentially interacted with ceria component on the surface of CZ; (2) for CuO/WO_3/CZ samples with a half-monolayer WO_3 loading, i.e., *x*Cu−0.4W−CZ series, the surface of CZ is only partially covered by the preloaded WO_3, and the supported copper oxide species are dispersed on the remaining surface vacant sites on CZ as well as on top of the preloaded tungsten oxide, while for the samples preloaded with a full-monolayer WO_3, i.e., *x*Cu−0.8W−CZ series, only dispersed on the top of the preloaded tungsten oxide monolayer; (3) the effect of the loading amount of WO_3 on the reduction property of Cu^{2+} ions in a series of CuO/WO_3/CZ samples has been observed and tentatively attributed to the formation of WO_3 monolayer on CZ and the different coordination environments of the dispersed Cu^{2+} ions are discussed on the basis of the consideration of the incorporation model proposed previously (Chen, Y.; Zhang, L. *Catal. Lett.* **1992**, *12,* 51).

Introduction

In recent research, studies on supported metal oxides, especially the multicomponent-supported catalysts have attracted much attention, due to their extensive use as heterogeneous catalysts in numerous chemical processes, such as the $CuO/CeO_2/TiO_2$ catalyst for the complete oxidation of CO, ethanol, and ethyl acetate; $V_2O_5-WO_3/TiO_2$ catalyst in the reduction of NO_x by NH_3 and WO_3-modified $NiO-ZrO_2$ for the dimerization of ethylene.[1−3]

Due to the complexity of the multicomponent-supported catalysts, though many correlative research studies have been carried out, there is still a lack of general agreement on the intrinsic interactions among the components.[4,5] For example, in $CuO/CeO_2/TiO_2$ catalysts, the interactions should involve all the species including dispersed copper oxide, crystalline copper oxide, dispersed ceria species, crystalline CeO_2, and TiO_2 support, etc.

The preparation and application of ceria−zirconia solid solution have been reported by many researchers.[6−8] On the basis of the excellent thermal stability and high OSC (oxygen storage capacity) of the solid solution in a wide range of ceria concentration,[9] ceria−zirconia mixed oxides have been used as an important component of the three-way catalysts for treating automotive exhaust gas with a great deal of advantages.[10,11] WO_3 is also an effective component in the selective catalytic reduction of NO_x by ammonia such as $V_2O_5-WO_3$ supported on TiO_2 anatase.[12] Additionally, tungsten-supported oxide can be used as precursors of corresponding supported sulfide in hydrodesulfurization (HDS).[13] CuO is widely used as active species in various catalytic processes and is considered to be a possible substitution of noble metal catalysts in many aspects.[14]

Studies on the properties of supported metal oxides and the interactions between the dispersed metal oxide species and supports are critical in getting a deeper understanding of the related catalytic behaviors. It is generally accepted that, on γ-Al_2O_3,[15,16] ZrO_2,[17,18] CeO_2,[19,20] and TiO_2,[21,22] when the loading of WO_3 (or CuO) is low enough, it exists in a highly dispersed monolayer-type structure, although the exact identity of this structure is still open for discussion. Comparatively, multicomponent-supported catalysts, especially with solid solution as a support, have received little attention in the past.

In the present work, the solid solution $Ce_{0.5}Zr_{0.5}O_2$, hereafter denoted as CZ, was used as support for the preparation of CuO/WO_3/CZ samples, and the studies have been mainly focused on attempting to (1) determine the dispersion capacity of WO_3 supported on CZ; (2) explore the importance of surface composition and/or surface structure of the support on the properties of the dispersed oxide by studying the variation of reduction behavior of CuO supported on CZ and on the tungsten oxide premodified CZ; (3) propose a possible surface model of copper oxides and tungsten oxide species on the surface of the support, discussed on the basis of the consideration of the incorporation model proposed previously.

Experimental Section

(1) Catalyst Preparation. $Ce_{0.5}Zr_{0.5}O_2$ solid solution was prepared by traditional co-precipitation method. $Ce(NO_3)_3$ and

* To whom correspondence should be addressed. Fax: 86-25-83317761. E-mail: donglin@nju.edu.cn.
[†] Department of Chemistry.
[‡] College of Chemistry and Chemical Engineering.

10.1021/jp046731t CCC: $30.25
Published on Web 02/09/2005

$Zr(NO_3)_4$ solution with a molar ratio of Ce/Zr = 1:1 were mixed and stirred for 1 h. Then ammonium hydroxide solution (25% ammonia) was added dropwise to the mixed solution until the pH value reached 10. The precipitation was kept at 100 °C for 12 h and then calcined in air at 600 °C for 8 h. XRD and LRS results showed that it was a homogeneous CeO_2-ZrO_2 solid solution with a cubic phase. The BET surface area was 50.8 m^2/g.

WO_3/CZ samples were prepared by impregnating CZ with an aqueous solution of ammonium metatungstate $[(NH_4)_6H_2W_{12}O_{40}]$ containing requisite amount of WO_3 followed by drying in air at 100 °C for 12 h and then calcining in air at 500 °C for 5 h, and these samples were denoted as W/CZ.

Samples of CuO supported on W/CZ were prepared by impregnating W/CZ supports with an aqueous solution containing the requisite amount of $Cu(NO_3)_2$. The samples were dried at 100 °C for 12 h and then calcined in oxygen at 450 °C for 5 h. The loading amount of CuO was calculated by referring to the original surface area of CZ in sample W/CZ. For simplicity, CuO/W/CZ samples were denoted as *x*Cu−*y*W−CZ, e.g. 0.4Cu−0.8W−CZ corresponds to a sample with CuO and WO_3 loading amounts of 0.4 and 0.8 mmol/(100 m^2 CZ), respectively. Similarly, *x*Cu−CZ represented a sample with copper oxide loading of *x* mmol/(100 m^2 supported on CZ).

WO_3 was obtained by calcining the commercial WO_3 sample in air at 500 °C for 5 h, and after calcinations its BET surface area was 9.7 m^2/g. For the CuO/WO_3 sample, prepared by impregnating WO_3 supports with an aqueous solution containing $Cu(NO_3)_2$, the weight percent of CuO was the same as that in the sample 0.8Cu−CZ. The sample was dried at 100 °C for 12 h and then calcined in oxygen at 450 °C for 5 h.

(2) Characterization. X-ray diffraction (XRD) patterns were obtained with a Philips X'pert Pro diffractometer using Ni-filtered Cu Kα radiation (0.154 18 nm). The X-ray tube was operated at 40 kV and 40 mA.

BET (Brunauer−Emmett−Teller) surface areas were measured by nitrogen adsorption at 77 K on a Micromeritics ASAP-2000 adsorption apparatus.

Laser Raman spectra (LRS) were recorded by using JOBIN-YVON T64000 Raman spectrometer. Raman excitation at 514.5 nm was provided by Ar^+ laser. A laser power of 300 mW at the sample was applied.

X-ray photoelectron spectroscopy (XPS) results were obtained by using a V. G. Escalab MK II spectrometer equipped with a hemispherical electron analyzer. The system was operated at 13 kV and 20 mA using a magnesium anode (Mg Kα, E = 1253.6 eV). A binding energy (BE) of 284.5 eV for the C 1s level was used as an internal reference.

Temperature-programmed reduction (TPR) was carried out in a quartz U-tube reactor, and a 100 mg sample was used for each measurement. Before reduction, the sample was pretreated in N_2 stream at 100 °C for 1 h and then cooled to room temperature. After that, a H_2-Ar mixture (7% H_2 by volume) was switched on and the temperature was increased linearly at a rate of 10 °C/min. A thermal conductivity cell was used to detect the consumption of H_2 on stream.

Results and Discussion

(1) Dispersion of WO_3 on $Ce_{0.5}Zr_{0.5}O_2$. Figure 1 shows the XRD patterns of a series of W/CZ samples with different WO_3 loadings. The XRD patterns of CZ and pure WO_3 are also presented for comparison. For samples with low WO_3 loading (≤0.8 mmol/(100 m^2 CZ)), i.e., Figure 1b,c with 0.4 and 0.8 mmol/(100 m^2 CZ), respectively, no characteristic peaks of crystalline WO_3 (typically at 2θ = 23.1, 23.64, and 24.36°) has been observed, which suggests that the tungsten oxide species have been highly dispersed on the surface of the CZ solid solution. However, characteristic peaks of crystalline WO_3 have been found in high WO_3 loading samples, i.e., Figure 1d−g, and the intensity of the peaks increases with the increase of the WO_3 loading, indicating the formation of crystalline WO_3 due to the high WO_3 loading amount in these samples.

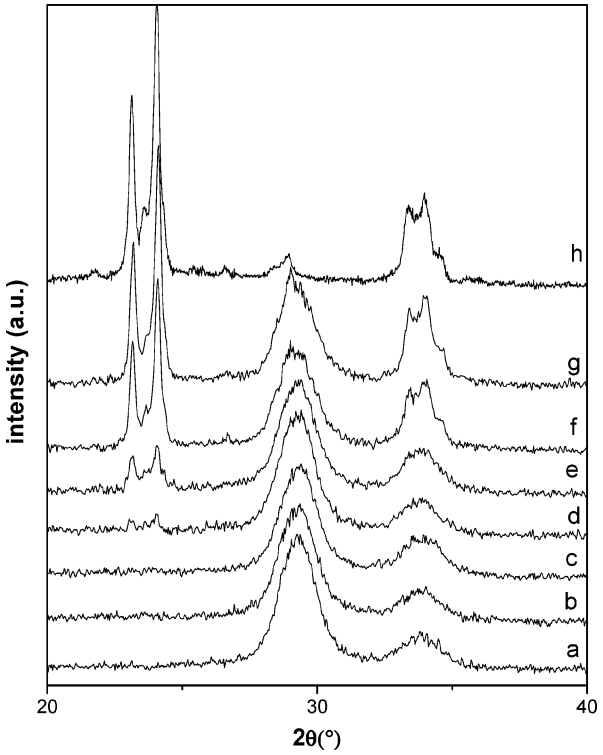

Figure 1. XRD patterns: (a) CZ; (b−g) W/CZ samples with WO_3 loadings of 0.4, 0.8, 1.2, 3.0, 6.0, and 8.0 mmol/(100 m^2 CZ), respectively; (h) WO_3.

XRD quantitative analysis is carried out by measuring the peak intensity ratios of crystalline WO_3 and CZ support as a function of tungsten oxide loading to determine the dispersion capacity of tungsten oxide supported on CZ.[23] The result is shown in Figure 2, the straight line corresponding to the formation of crystalline WO_3 does not go through the origin but cuts an intercept on the abscissa at a value which is referring to the dispersion capacity of WO_3 on CZ. Accordingly, the dispersion capacity of tungsten oxide on CZ is around 0.8 mmol/(100 m^2).

The BET results of W/CZ samples with different WO_3 loadings are listed in Table 1. Increasing WO_3 loading from 0 to 0.8 mmol/(100 m^2 CZ), the BET surface area decreases slowly from 50.8 to 42.3 m^2/g, and when the WO_3 loading increases to 1.2 mmol/(100 m^2), the surface area drops dramatically to 33.8 m^2/g due to the formation of a crystalline WO_3 phase.

LRS is a powerful characterization technique for obtaining detailed information about the structure of supported metal oxide, especially high-valence metal oxides, such as MoO_3, WO_3, and V_2O_5, etc, because the dispersed metal oxide species have a vibration spectrum different from those of the crystal species or amorphous form. Figure 3 shows laser Raman spectra ranging from 200 to 1100 cm^{-1} of W/CZ with different WO_3 loadings; pure WO_3 is also included for comparison. In spectrum e, the bands around 713 and 806 cm^{-1}, characteristic peaks of the crystalline WO_3,[16] are detected. In low WO_3 loading samples (≤0.8 mmol(/100 m^2 CZ)), i.e., spectra a and b, only the band

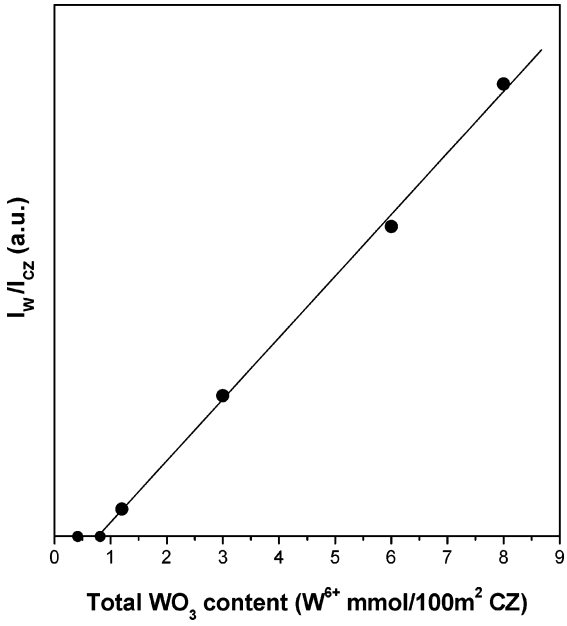

Figure 2. Relationship between I_W/I_{CZ} and WO_3 loading in W/CZ samples.

TABLE 1: BET Results of a Series of W/CZ Samples with Different WO_3 Loadings

WO_3 loading amount (mmol/(100 m^2))	BET surface area (m^2/g)
0	50.8
0.4	46.4
0.8	42.3
1.2	33.8

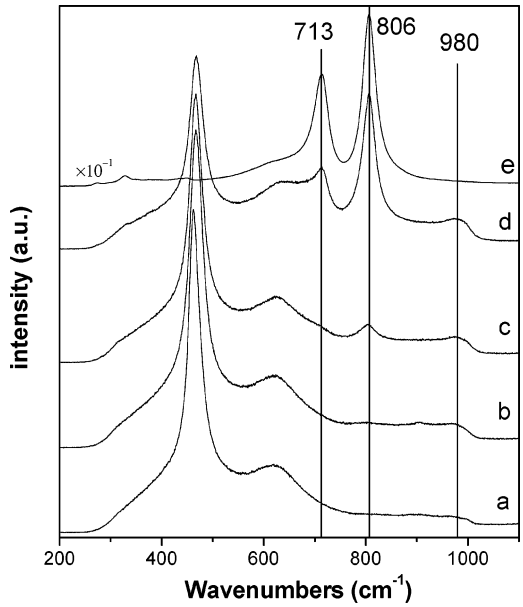

Figure 3. Raman spectra: (a−d) W/CZ samples with WO_3 loadings of 0.4, 0.8, 1.2, and 3.0 mmol/(100 m^2 CZ), respectively; (e) WO_3.

around 980 cm^{-1} is found, which may attribute to the symmetrical W═O stretching mode of the dispersed tungsten oxide species on the surface of support,[16] and the intensity of the band increases with the increase of the WO_3 loading, indicating that tungsten oxides are highly dispersed on CZ. For spectra c and d, the crystalline WO_3 bands (713 and 806 cm^{-1}) appear, and their intensities increase with the WO_3 loading; in contrast, no obvious change can be seen in the band around 980 cm^{-1}, suggesting that the amount of the dispersed tungsten oxide species has reached a fixed value in them.

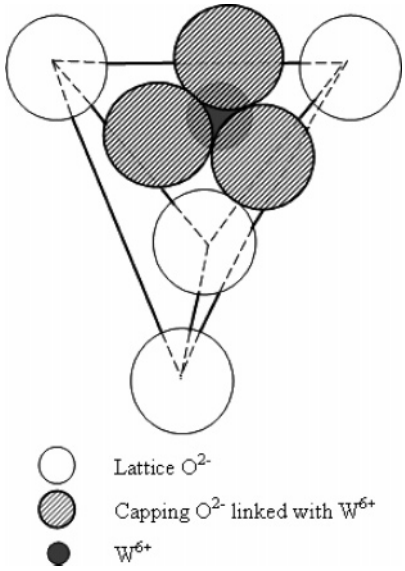

Figure 4. Tentative model of the surface WO_3 species dispersed on the (111) plane of the CZ support.

The above BET and LRS results are consistent with the XRD quantitative analysis that the dispersion capacity of tungsten oxide on CZ is around 0.8 mmol/(100 m^2).

As discussed elsewhere, the (111) plane with cubic vacant sites is preferentially exposed on the surface of CeO_2 and ZrO_2; both of these two metal oxides have a fluorite structure.[24,25] It seems reasonable to tentatively suggest that the (111) plane is also preferentially exposed on the surface of CZ, the solid solution of CeO_2 and ZrO_2, which has a fluorite structure as well. Accordingly, the dispersion capacity of WO_3 on CZ as well as the configuration of the highly dispersed WO_3 species can be estimated by using the incorporation model proposed previously.[26] It is suggested that similar to the case of the dispersion of WO_3 on ceria,[20,27] the number of the vacant sites on CZ is about 1.22 mmol/(100 m^2) and the incorporated W^{6+} ion should have an asymmetric seven-coordination surrounding, as shown in Figure 4, similar to that of WO_3 highly dispersed on CeO_2.[20] As each incorporated W^{6+} ion is accompanied by three oxygen capping anions for charge compensation, the shielding effect produced by these capping anions prevents some of the neighboring vacant sites on CZ from being incorporated by other tungsten ions. The value of dispersion capacity can be deduced by calculation that upon WO_3 reaching its dispersion capacity, the oxygen anions accompanied with the incorporated W^{6+} ions forming a close-parked monolayer on the surface of CZ with some still unoccupied vacant sites underneath.[21,28] The value 0.82 mmol/(100 m^2) thus estimated matches well with that obtained by XRD.

(2) Dispersion and Reduction of CuO on the WO_3-Modified $Ce_{0.5}Zr_{0.5}O_2$. *(2.1) Dispersion of CuO on the WO_3-Modified $Ce_{0.5}Zr_{0.5}O_2$.* Figure 5 shows the XRD patterns of *x*Cu−0.4W−CZ and *x*Cu−0.8W−CZ series samples. The results indicate that the copper oxide exists as highly dispersed species when the CuO loading is 0.4 mmol/(100 m^2), as can be seen in the samples 0.4Cu−0.4W−CZ and 0.4Cu−0.8W−CZ. When the CuO loading is 0.8 mmol/(100 m^2), as observed in 0.8Cu−0.4W−CZ and 0.8Cu−0.8W−CZ samples, the existence of crystalline CuO is obvious, and their peak intensities increase with the increase of CuO loading.

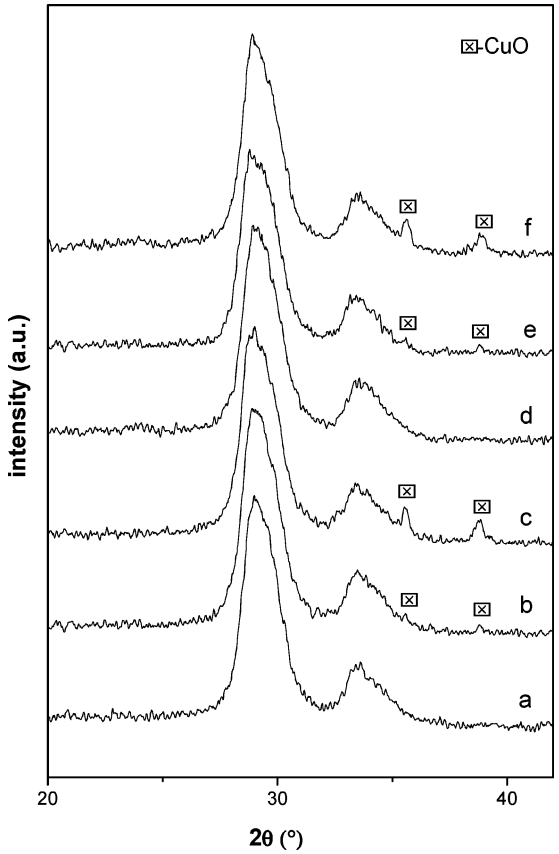

Figure 5. XRD patterns of *x*Cu−0.4W−CZ and *x*Cu−0.8W−CZ samples: (a) 0.4Cu−0.4W−CZ; (b) 0.8Cu−0.4W−CZ; (c) 2.0Cu−0.4W−CZ; (d) 0.4Cu−0.8W−CZ; (e) 0.8Cu−0.8W−CZ; (f) 2.0Cu−0.8W−CZ.

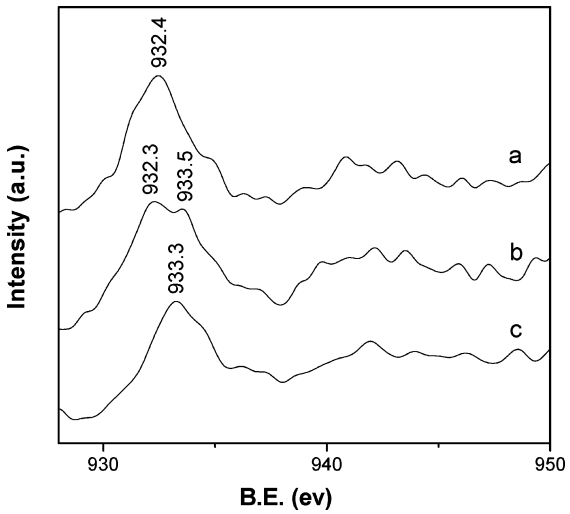

Figure 6. Cu $2p_{3/2}$ XPS spectra of 0.4Cu−*x*W−CZ samples: (a) 0.4Cu−CZ; (b) 0.4Cu−0.4W−CZ; (c) 0.4Cu−0.8W−CZ.

To further investigate the surface properties of the CuO/W/CZ samples, XPS profiles of the 0.4Cu−xW−CZ series samples are measured and shown in Figure 6, from which one can see that the BE of Cu $2p_{3/2}$ of the 0.4Cu−CZ sample is 932.4 eV, which is much lower than that of crystalline CuO (i.e. 933.6 eV[29]). This should be related to the different coordination environment of copper species. For crystalline CuO, Cu^{2+} ion is located on distorted octahedral sites with a coordination number of 6, while for 0.4Cu−CZ, copper oxide is highly dispersed on the surface of CZ, and Cu^{2+} ion may be located

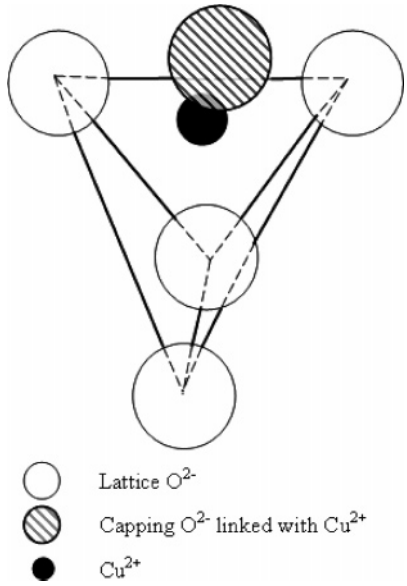

Figure 7. Tentative model of surface five-coordinated Cu^{2+} species formed by incorporating of Cu^{2+} ion into the surface cubic vacant sites of CZ.

in the vacant site with a coordination of five oxygen ions similar to the dispersion of CuO on CeO_2,[19] as shown in Figure 7. For the case of the 0.4Cu−0.4W−CZ sample one can see a shoulder peak at 933.5 eV appears beside the peak at 932.4 eV and noteworthy only the 933.5 eV peak can be observed in the 0.4Cu−0.8W−CZ sample, in which, as discussed previously, the loading amount of WO_3 has reached the theoretical value and is just enough to form a complete monolayer of WO_3 on CZ. Taking into consideration the fact that XRD did not detect the existence of any CuO crystalline in this sample, it seems reasonable to consider that the supported CuO species are highly dispersed on the WO_3 monolayer preloaded on CZ and responsible for the peak with the BE of 933.3 eV. Along this line, the existence of two peaks in the XPS spectrum of the 0.4Cu−0.4W−CZ sample is natural as, in which the preloaded amount of WO_3 is only the half for the formation of a complete monolayer, the supported CuO species should disperse both on the preloaded WO_3 (933.5 eV) as well as on CZ (932.4 eV). The above results reveal that the dispersion properties of copper oxide species on CZ are strongly influenced by its modification of the preloaded WO_3 species.

The surface Ce/Zr ratio of a series of samples evaluated from their XPS profiles are shown in Figure 8. It is interesting to see that there is a decrease of the Ce/Zr ratio with the increase of WO_3 loading in the samples of b to c, and the result seems to indicate that the presence of WO_3 has a larger effect on decreasing the surface exposure possibility of Ce than that of Zr. In other words, relatively more surface Ce than Zr species are covered by the supported WO_3; the result is in agreement with the fact that WO_3 is an acidic oxide and the basicity of CeO_2 is stronger than ZrO_2.[30,31] Accordingly the supported tungstic oxide species should preferentially interact with ceria instead of zircornia species on the surface of CZ, and the distribution of these species is schematically shown in Figure 8. From Figure 9, one can see that the BE of O 1s in these samples is increased with the WO_3 loading, which might attribute to the larger electronegativity of W^{6+} in comparison with those of Zr^{4+} and Ce^{4+}.[32] Consequently the presence of more dispersed tungstic oxide species tends to pull more electron from oxygen anions on the surface, leading to a shift of the O 1s peak to higher binding energy.

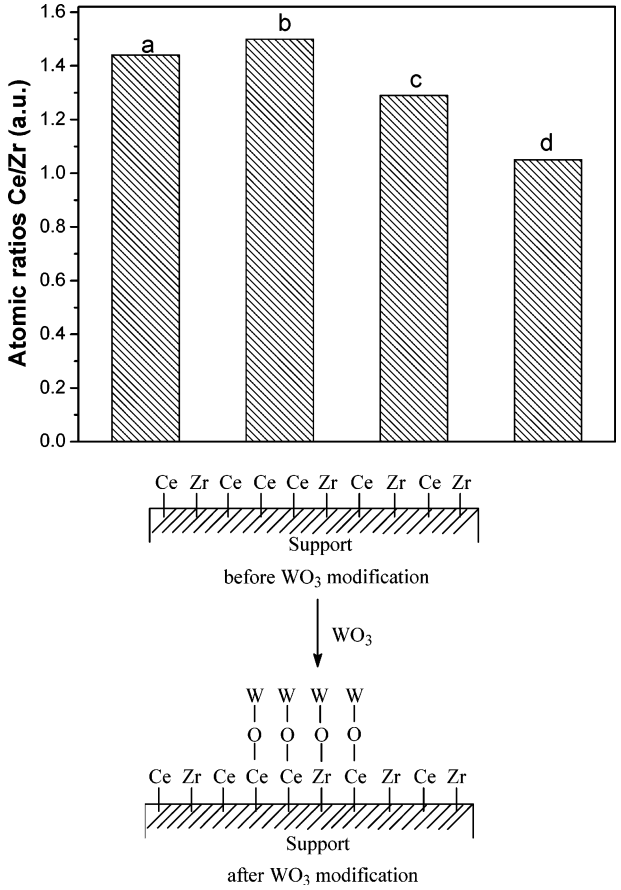

Figure 8. (Top panel) Surface atomic ratios of Ce/Zr from XPS results: (a) CZ; (b) 0.4Cu−CZ; (c) 0.4Cu−0.4W−CZ; (d) 0.4Cu−0.8W−CZ. (Bottom panel) Schematic diagram of the distribution of tungstic oxide species on the surface of $Ce_{0.5}Zr_{0.5}O_2$.

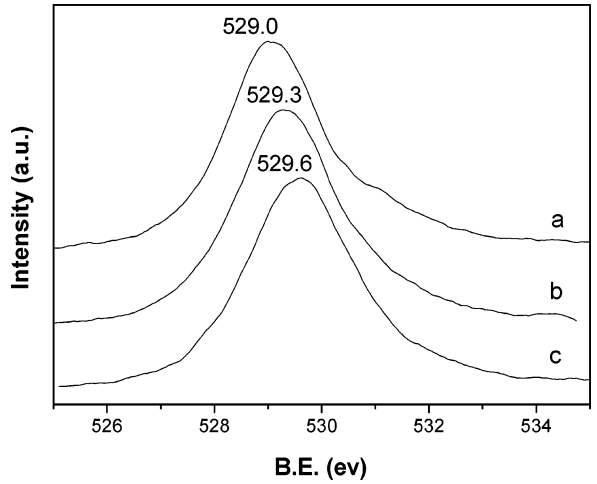

Figure 9. O 1s XPS spectra of 0.4Cu−*x*W−CZ samples: (a) 0.4Cu−CZ; (b) 0.4Cu−0.4W−CZ; (c) 0.4Cu−0.8W−CZ.

(2.2) Reduction Behaviors of CuO on the WO_3-Modified $Ce_{0.5}Zr_{0.5}O_2$. (2.2.1) Reduction Properties of CuO on Samples with the Same Loading of WO_3. Complemental experiments have shown that the TPR profiles of all W/CZ samples only show a reduction peak at temperatures higher than 500 °C; hence, the peaks below 500 °C detected in TPR profiles of the CuO/W/CZ samples should be related to the reduction of copper oxide species.

Shown in Figure 10 are the TPR profiles of *x*Cu−CZ and *x*Cu−0.4W−CZ series samples; the loading amounts of WO_3 in the *x*Cu−0.4W−CZ series samples are identical, i.e., 0.4 mmol WO_3/(100 m^2 CZ), about half of its dispersion capacity.

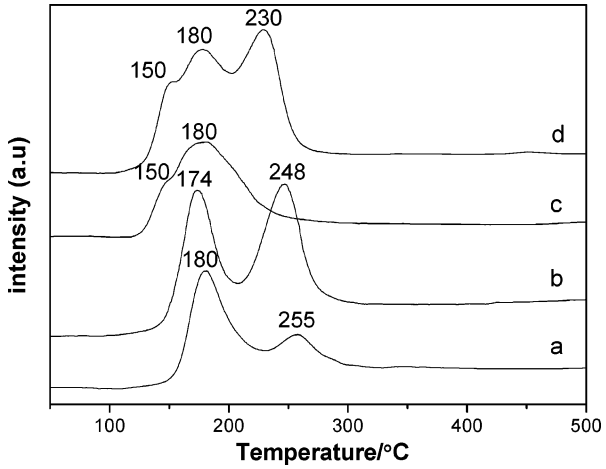

Figure 10. TPR profiles of *x*Cu−0.4W−CZ and *x*Cu−CZ samples: (a) 0.8Cu−0.4W−CZ; (b) 2.0Cu−0.4W−CZ; (c) 0.8Cu−CZ; (d) 2.0Cu−CZ.

For CuO/CZ samples, i.e., curves c and d, the peaks at about 150 and 180 °C are attributed to the stepwise reduction of surface dispersed CuO species, i.e., $Cu^{2+}\rightarrow Cu^{+}$ and $Cu^{+}\rightarrow Cu^{0}$, and the peak at 230 °C is due to the reduction of crystalline CuO, which is similar to the reduction of CuO dispersed on CeO_2 reported elsewhere.[19,33] In contrast, only two reduction peaks are found in the TPR profiles of the *x*Cu−0.4W−CZ samples, i.e., curves a and b, one at about 180 °C assigned to the reduction of dispersed CuO species and the other at about 250 °C attributed to the reduction of crystalline CuO. These facts indicate that, as an explanation, the existence of dispersed WO_3 species might induce the reduction of dispersed CuO from two steps to one step.

As shown in the XRD results of Figure 5, characteristic crystalline CuO peaks are found in the 0.8Cu−0.4W−CZ sample, and the intensity of these diffraction peaks is increased in sample 2.0Cu−0.4W−CZ, which has a higher CuO loading than that of 0.8Cu−0.4W−CZ. For TPR profiles a and b in Figure 10, the area of the peak at about 250 °C also increases with the content of CuO, while the peak at about 180 °C keeps almost unchanged. These results reveal that the two peaks are due to the reduction of crystalline and dispersed CuO species, respectively. No crystalline CuO is observed in the 0.8Cu−CZ sample since the loading amount is less than the dispersion capacity of CuO supported on CZ, which is about 1.2 mmol/(100 m^2) evaluated from the incorporation model. For the case of CuO supported on W/CZ, as some of the vacant sites on the surface of CZ are occupied by the preloaded WO_3 species, comparatively crystalline CuO shows up at a lower copper oxide loading. The TPR profiles of the two *x*Cu−0.8W−CZ samples shown in Figure 11 are similar to that of *x*Cu−0.4W−CZ. The peak around 290 °C in both profiles a and b should be assigned to the reduction of crystalline CuO, and the one around 195 °C, to the reduction of dispersed CuO species.

(2.2.2) Influence of WO_3 Loading Amount on the Reduction of CuO. The TPR profiles of 0.8Cu−*x*W−CZ samples are shown in Figure 12. It is noticeable that the reduction temperature of dispersed CuO is changed with WO_3 loadings. For 0.8Cu−0.4W−CZ sample, the loading amount of WO_3 is about a half-monolayer and the reduction peak of dispersed CuO species is about 180 °C, while, for the sample with a full monolayer of WO_3 loading preloaded (0.8Cu−0.8W−CZ), the peak shifts to 200 °C. This phenomenon could be explained as

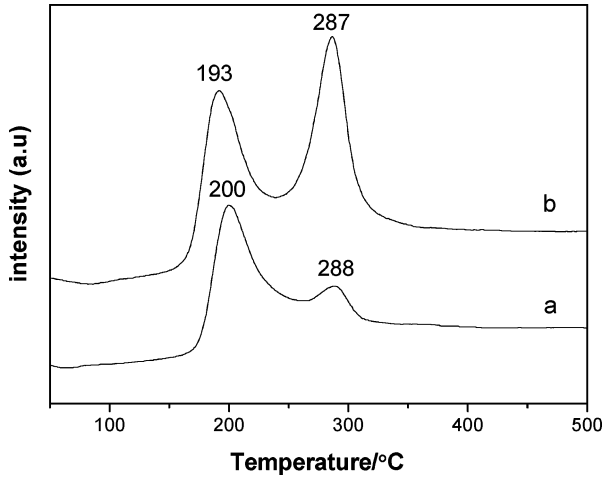

Figure 11. TPR profiles of *x*Cu−0.8W−CZ samples: (a) 0.8Cu−0.8W−CZ; (b) 2.0Cu−0.8W−CZ.

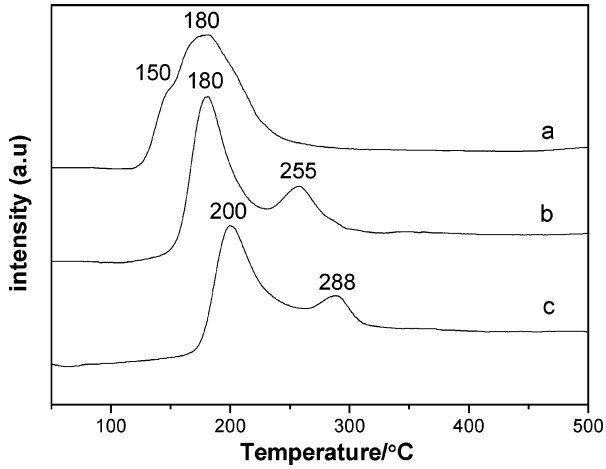

Figure 12. TPR profiles of 0.8Cu−*x*W−CZ samples: (a) 0.8Cu−CZ; (b) 0.8Cu−0.4W−CZ; (c) 0.8Cu−0.8W−CZ.

follows: in samples with a half-monolayer WO_3 preloaded, there are still vacant sites left on the surface of CZ for the dispersion of CuO, while, for samples preloaded with a full monolayer WO_3, the surface of CZ is fully covered with a complete monolayer of WO_3 species and the added Cu^{2+} can only disperse on the surface of the WO_3 monolayer. The result is also supported by the XPS results mentioned above. This phenomenon is somewhat different from the results in the $ZnO/MoO_3/t\text{-}ZrO_2$ system reported previously.[34] When Cu^{2+} ion is incorporated into the surface cubic vacant site of CZ, it could be considered that the Cu^{2+} ion is in a five-coordination environment, as shown in Figure 7. When Cu^{2+} ion is incorporated into the vacant site on the close-packed monolayer of dispersed WO_3 species, four O^{2-} ions are around each Cu^{2+} ion: three O^{2-} ions linked with W^{6+} and the capping O^{2-} associated with Cu^{2+}, so the Cu^{2+} ion should have a tetrahedral coordination environment (Figure 13). Compared with the five-coordination environment, Cu^{2+} in a tetrahedral coordination environment should be more stable due to its higher symmetry and needs higher temperature to be reduced. Thus, the reduction temperature of dispersed CuO in samples preloaded with half-monolayer WO_3 is lower than that in samples preloaded with full-monolayer WO_3.

It is interesting to note that the reduction temperature of crystalline CuO is also different with the variation of WO_3 loadings, as shown in the reduction of 2.0Cu−*x*W−CZ samples in Figure 14. For sample 2.0Cu−CZ, the reduction peak of

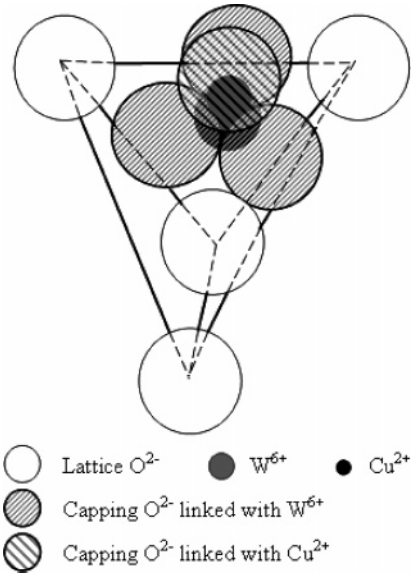

Figure 13. Tentative model of surface tetrahedral coordination Cu^{2+} species formed by incorporation of Cu^{2+} ion into the surface vacant sites of the dispersed WO_3 monolayer.

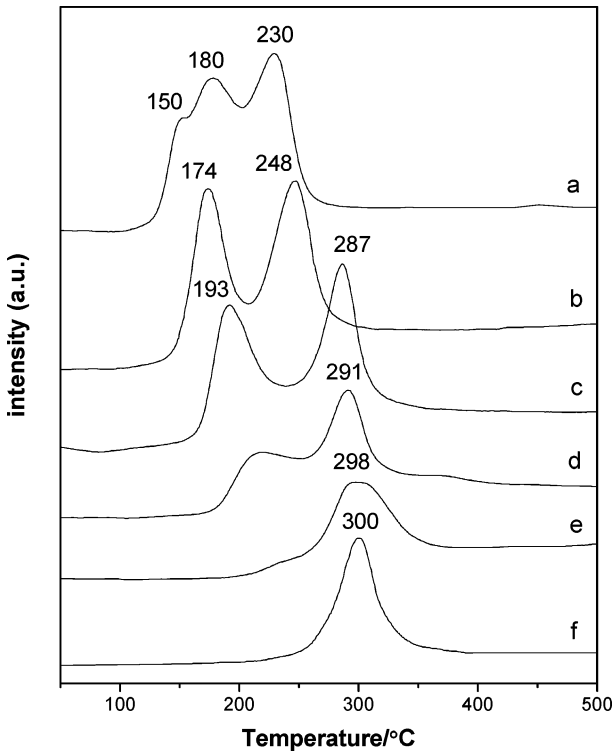

Figure 14. TPR profiles of 2.0Cu−*x*W−CZ samples: (a) 2.0Cu−CZ; (b) 2.0Cu−0.4W−CZ; (c) 2.0Cu−0.8W−CZ; (d) 2.0Cu−3.0W−CZ; (e) CuO/WO_3; (f) CuO.

crystalline CuO is at about 230 °C, while, in 2.0Cu−0.4W−CZ, it shifts toward higher temperature region and reaches 248 °C. As the amount of the preloaded WO_3 exceeds its dispersion capacity, such as in samples 2.0Cu−0.8W−CZ and 2.0Cu−3.0W−CZ, the reduction peak of crystalline CuO reaches a value of about 290 °C. For the case of the CuO/WO_3 sample, the surface area of WO_3 is rather small: only a little amount of CuO can be dispersed on it, reflecting in a small shoulder peak observed in the TPR profile before 250 °C; however, a large peak, assigned to the reduction of crystalline CuO, centered around 290−300 °C can clearly be seen. The result is similar to that observed in 2.0Cu−0.8W−CZ and 2.0Cu−3.0W−CZ

samples. Unsupported CuO also has the single reduction peak centered at 300 °C. Combining the above results, it seems that, in common, when the amount of the preloaded WO_3 exceeds its dispersion capacity, the reduction peak of crystalline CuO shifts to a higher temperature. Similarly, for CuO/CeO_2 samples, the reduction temperature of crystalline CuO in high CuO loading samples is also lower than unsupported CuO.[19,35] Zimmer suggests that the hydrogen adsorbed on active sites of the cerium oxide surface might accelerate the reduction of the supported crystalline CuO.[33] For *x*Cu−0.8W−CZ or higher tungsten oxide containing samples, it seems reasonable to suggest that the close-packed monolayer of the preloaded WO_3 might inhibit the interaction between CuO species and the surface of CZ, and consequently, the reduction temperature of crystalline CuO in samples 2.0Cu−0.8W−CZ and 2.0Cu−3.0W−CZ is higher than that in 2.0Cu−CZ and 2.0Cu−0.4W−CZ, but similar to unsupported CuO.

Conclusions

Quantitative XRD, BET, and LRS results reveal that WO_3 can highly disperse on the surface of $Ce_{0.5}Zr_{0.5}O_2$, denoted as CZ, solid solution with a dispersion capacity around 0.8 mmol/(100 m^2), which is consistent with the value expected by the incorporation model, and it is suggested that the dispersed W^{6+} ion is in a seven-coordination environment and preferentially interacts with surface ceria species of CZ.

The surface property of the support can be modified to different extent, depending on the loading amount of WO_3. It is suggested that when CuO is supported on WO_3/CZ with its WO_3 content about of a half-monolayer, Cu^{2+} ions are partially dispersed on the uncovered surface vacant sites on CZ in a five-coordination environment as well as on the top of the preloaded WO_3 species, and when the WO_3 loading reaches to its dispersion capacity on CZ, the supported Cu^{2+} can only disperse on top of the preloaded WO_3 monolayer, locating in a tetrahedral coordination environment. It is tentatively suggested that for the highly dispersed Cu^{2+} ions, the influence of the WO_3 on their reduction temperature is related to the different coordination environments of the Cu^{2+} ions caused by the existence of the WO_3, while for the case of supported crystalline CuO to the formation of the interlayer of the preloaded WO_3, which covers the surface of CZ to a certain extent.

Acknowledgment. The financial support of the Science and Technology Funding of Jiang-su Province, China (Grant No. BG2001038), the Specialized Research Fund for the Doctoral Program of Higher Education (Grant No. 20030284002), and the National Basic Research Program of China (Grant No. 2003CB615804) is gratefully acknowledged.

References and Notes

(1) Larsson, P.; Andersson, A. *J. Catal*. **1998**, *179*, 72.
(2) Lietti, L. *Appl. Catal., B* **1996**, *10*, 281.
(3) Sohn, J. R.; Lee, S. Y. *Appl. Catal., A* **1997**, *164*, 127.
(4) Matralis, H. K.; Ciardelli, M.; Ruwet, M.; Grange, P. *J. Catal.* **1995**, *157*, 368.
(5) Ramirez, J.; Gutierrez-Alejandre, A. *J. Catal*. **1997**, *170*, 108.
(6) Sato, T.; Dosaka, K.; Ishitsuka, M.; Haga, E. M.; Okuwaki, A. *J. Alloys Compd.* **1993**, *193*, 274.
(7) Fegley, B.; Barringer, A. *Mater. Res. Soc. Symp. Proc.* **1984**, *32*, 187.
(8) Tani, E.; Yoshimura, M.; Somiya, S. *J. Am. Ceram. Soc*. **1983**, *66* (7), 506.
(9) Ozawa, M.; Kimura, M.; Isogai, A. *J. Alloys Compd.* **1993**, *193*, 73.
(10) Leitenburg, C.; Trovarelli, A.; Zamar, F.; Maschio, S.; Dolcetti, G.; Llorca, J. *J. Chem. Soc., Chem. Commun.* **1995**, 2181.
(11) Murota, T.; Hasegawa, T.; Aozasa, S.; Matsui, H.; Motoyama, M. *J. Alloys Compd.* **1993**, *193*, 298.
(12) Alemany, L. J.; Berti, E.; Busca, G.; Ramis, G.; Robba, D.; Toledo, G. P.; Trombetta, M. *Appl. Catal., B* **1996**, *10*, 299.
(13) Chianelli, R. R.; Daage, M.; Ledoux, M. *J. Adv. Catal*. **1994**, *40*, 177.
(14) Kummer, J. T. *Prog. Energy Combust. Sci.* **1980**, *6*, 177.
(15) Hu, Y. H.; Dong, L.; Wang, J.; Ding, W. P.; Chen, Y. *J. Mol. Catal. A: Chem.* **2000**, *162*, 307.
(16) Wachs, I. E.; Murrell, L. L. *J. Catal.* **1984**, *90*, 150.
(17) Zhou, R. X.; Yu, T. M.; Jiang, X. Y.; Chen, F.; Zheng, X. M. *Appl. Surf. Sci.* **1999**, *148*, 263.
(18) Di Gregorio, F.; Keller, V. *J. Catal.* **2004**, *225*, 45.
(19) Dong, L.; Jin, Y. S.; Chen, Y. *Sci. China, Ser. B: Chem., Life Sci., Earth Sci.* **1997**, *40*, 24.
(20) Dong, L.; Hu, Y. H.; Xu, F.; Lu, D.; Xu, B.; Hu, Z.; Chen, Y. *J. Phys. Chem. B* **2000**, *104*, 78.
(21) Xu, B.; Dong, L., Chen, Y., Xu, B.; Dong, L.; Chen, Y. *J. Chem. Soc., Faraday Trans.* **1998**, *94*, 1905.
(22) Xu, B.; Dong, L.; Fan, Y. N.; Chen, Y. *J. Catal.* **2000**, *193*, 88.
(23) Xie, Y. C.; Tang, Y. Q. *Adv. Catal*. **1990**, *37*, 1.
(24) Cochrane, H. D.; Hutchison, J. L. *Ultramicroscopy* **1989**, *31*, 138.
(25) Liu, Z.; Chen, Y. *J. Catal.* **1998**, *177*, 314.
(26) Chen, Y.; Zhang, L. F. *Catal. Lett.* **1992**, *12*, 51.
(27) Dong, L.; Chen, Y. *Chin. J. Catal*. **1995**, *16* (2), 85.
(28) Dong, L.; Chen, Y. *J. Chem. Soc., Faraday Trans.* **1996**, *92*, 4589.
(29) Wagner, C. D.; Riggs, W. M.; Davis, L. E.; Moulder, J. F.; Muilenberg, G. E. *Handbook of X-ray Photoelectron Spectroscopy*; Perkin-Elmer: Palo Alto, CA, 1978.
(30) Waqif, M.; Saad, A. M.; Bensitel, M.; Bachelier, J.; Saur, O.; Lavalley, J. C. *J. Chem. Soc., Faraday Trans.* **1992**, *88*, 2931.
(31) Ziolek, M.; Kujawa, J.; Saur, O.; Lavalley, J. C. *J. Phys. Chem.* **1993**, *97*, 9761.
(32) Dean, J. A. *Lange's Handbook of Chemistry*, 15th ed.; McGraw-Hill Book Co.: Singapore, 1999; p 4.29.
(33) Zimmer, P.; Tschope, A.; Birringer, R. *J. Catal.* **2002**, *205*, 339.
(34) Liu, Z.; Dong, L.; Ji, W. J.; Chen, Y. *J. Chem. Soc., Faraday Trans.* **1998**, *94*, 1137.
(35) Jiang, X. Y.; Lu, G. L.; Zhou, R. X.; Mao, J. X.; Chen, Y.; Zheng, X. M. *Appl. Surf. Sci.* **2001**, *173*, 208.